Ground motions on rocky, cliffed, and sandy shorelines generated by ocean waves

Adam P. Young,[1] Robert T. Guza,[1] Mark E. Dickson,[2] William C. O'Reilly,[1] and Reinhard E. Flick[1]

Received 28 February 2013; revised 22 October 2013; accepted 29 October 2013; published 5 December 2013.

[1] We compare ground motions observed within about 100 m of the waterline on eight sites located on shorelines with different morphologies (rock slope, cliff, and sand beaches). At all sites, local ocean waves generated ground motions in the frequency band 0.01–40 Hz. Between about 0.01 and 0.1 Hz, foreshore loading and gravitational attraction from ocean swell and infragravity waves drive coherent, in-phase ground flexing motions mostly oriented cross-shore that decay inland. At higher frequencies between 0.5 and 40 Hz, breaking ocean waves and wave-rock impacts cause ground shaking. Overall, seismic spectral shapes were generally consistent across shoreline sites and usually within a few orders of magnitude despite the diverse range of settings. However, specific site response varied and was influenced by a combination of tide level, incident wave energy, site morphology, ground composition, and signal decay. Flexing and shaking increased with incident wave energy and was often tidally modulated, consistent with a local generation source. Flexing magnitudes were usually larger than shaking, and flexing displacements of several mm were observed during relatively large incident wave conditions (Hs 4–5 m). Comparison with traffic noise and earthquakes illustrate the relative significance of local ocean-generated signals in coastal seismic data. Seismic observations are not a simple proxy for wave-cliff interaction.

Citation: Young, A. P., R. T. Guza, M. E. Dickson, W. C. O'Reilly, and R. E. Flick (2013), Ground motions on rocky, cliffed, and sandy shorelines generated by ocean waves, *J. Geophys. Res. Oceans*, *118*, 6590–6602, doi:10.1002/2013JC008883.

1. Introduction

[2] Recent seismic observations at coastal cliffs suggest ground motions generated by local ocean waves may provide a convenient proxy for wave impacts on the cliff and improve our understanding of coastal processes. Cliff ground motion is elevated above background levels by different mechanisms in two general frequency bands. Higher frequency cliff motion (>0.3 Hz) or "shaking" can be generated from ocean waves directly impacting the cliff [*Adams et al*., 2002] or fronting shore platforms [*Dickson and Pentney*, 2012]. Low-frequency cliff motion (0.01–0.1 Hz) or "flexing" is generated as individual sea swell or single frequency waves [*Adams et al*., 2005] and infragravity waves [*Young et al*., 2011, 2012] load the foreshore, causing pressure fluctuations, combined with gravitational attraction of the ocean wave mass [*Agnew and Berger*, 1978]. Cliff flexing consists of downward and seaward translation and seaward ground tilt during wave loading, and vice versa during wave unloading. Previous studies show cliff shaking and flexing generally increases with incident wave height and water levels, but exceptions related to coastal setting have been observed [*Dickson and Pentney*, 2012].

[3] Observations of coastal ground motions are mostly limited to a few coastal cliffs and it is unknown if different coastal settings exhibit similar responses. Here, we compare near-shoreline ground motion observations at sandy beaches, and on top of cliffs fronted by beaches, elevated platforms, and by submerged platform/reef structures. Results from seven of the eight shoreline sites discussed are new, and include the first concurrent observations of ocean wave heights and ground motions on sandy beaches. The range of coastal settings is used to explore site ground motion generation and response related to varying coastal, geologic, and oceanographic settings. To place the results in context, the ocean-generated coastal ground motions are compared with two earthquakes and traffic noise from a nearby highway.

2. Background

[4] The limited number of previous studies of coastal ground motion has found that local ocean waves generate significant (above background levels) ground motion.

[1]Integrative Oceanography Division, Scripps Institution of Oceanography, University of California San Diego, La Jolla, California, USA.
[2]School of Environment, University of Auckland, Auckland, New Zealand.

Corresponding author: A. P. Young, Integrative Oceanography Division, Scripps Institution of Oceanography, University of California San Diego, 9500 Gilman Dr., La Jolla, CA 92093-0209, USA. (adyoung@ucsd.edu)

2169-9275/13/10.1002/2013JC008883

These studies have observational periods of a few months or less, and focus on frequencies ranging from 0.01 to 100 Hz. Various mechanisms have been suggested for generating ground motion, but as yet there is no consensus on what influences and/or controls the coastal seismic response to local wave forcing.

[5] *Bossolasco et al*. [1973] compared observations on top of an ocean-front cliff and a site a few km inland composed of hard ground covered by a thin surface layer of alluvium, on the inland side of a harbor. At the coastal cliff, the spectral densities (i.e., energy level) of single and double frequency motions were approximately equal. At the harbor site, single frequency motions were weaker, ascribed to reduced ocean wave energy within the structurally protected harbor.

[6] *Adams et al*. [2002] studied ground motion on top of a 10 m high central California cliff composed of Miocene mudstone capped by Quaternary marine terrace deposits, and fronted by a gently sloping submerged shore platform. They showed high frequency (1–25 Hz) wave-induced cliff shaking depended on offshore wave conditions, shelf bathymetry, and tide level. The high frequency shaking from wave impacts is accompanied by downward and seaward cliff flexing as incoming sea swell wave crests approach the cliff [*Adams et al*., 2005]. Observations at the cliff edge, 12 m and 30 m inland show cliff flexing decreased with increasing distance landward from the cliff edge. *Adams et al*. [2005] hypothesized that the associated strains generated by the inland decay of ground motion potentially reduce the material strength of coastal cliffs through fatigue; however, the plausibility of this mechanism is yet to be tested.

[7] *Dickson and Pentney* [2012] observed ground motion in the 1–100 Hz range along a cross-shore transect with seismometer positions at the cliff top edge, 50 m and 200 m inland, and at the base of a 37 m high cliff in New Zealand. The cliff was composed of consolidated sedimentary rocks, and fronted by an elevated (near mean high water) shore platform. Similar to previous studies, cliff ground motions increased with increasing incident wave height, decreased with distance inland, and were tidally modulated. However, in contrast with *Adams et al*. [2002, 2005], *Dickson and Pentney* [2012] found that during large wave events, cliff top ground motion was lowest at high tide and greatest at mid-low tide, suggesting the cliff top motion was enhanced by wave energy dissipated at the seaward edge of the elevated shore platform. Distinct water levels were also associated with an elevated cliff response at North Yorkshire, UK [*Lim et al*., 2011], suggesting a local topographic (e.g., platform morphology, and/or structural) influence. Additional seismic studies of coastal cliffs [*Amitrano et al*., 2005; *Senfaute et al*., 2009] focused on nonocean related signals including high frequency (40 Hz–10 kHz) seismic precursory patterns of cliff cracking and failure. At much lower frequencies (0.001–0.01 Hz, periods of 100–1000 s), *Agnew and Berger* [1978] suggested that the pressure loading and gravitational attraction of low-frequency ocean waves cause vertical ground motions at coastal sites, including a southern California coastal cliff. *Amundson et al*. [2012] observed ground tilt at coastal seismometers from long-period ocean waves (120–1200 s) and seiches generated by calving of the Greenland ice sheet. *Bromirski and Stephen* [2012] observed elevated local seismic signals related to ocean wave impacts on ice shelves.

[8] *Young et al*. [2011] compared ground motions at the frequencies of ocean infragravity and swell waves (between 0.01 and 0.1 Hz) on top of a coastal cliff in southern California with inland ground motions and cliff base water level fluctuations. At high tide, cliff top ground displacement magnitudes were coherent and in phase with water level fluctuations at the cliff base, and spectral levels at the cliff top were much higher than at the inland seismometer. At low tide, when ocean waves did not reach the cliff base, spectral levels of cliff ground motions decreased to inland levels at incident wave frequencies and higher, and only infragravity-band motions were noticeably forced by local ocean waves. At the same location, *Young et al*. [2012] investigated ground motions along a cross-shore transect and found vertical ground motions at infragravity and single frequencies decayed rapidly with inland distance from the cliff edge (*e*-folding scale is about 12 m), and at the edge decrease by several orders of magnitude between high tide and low tide. At approximately constant distance from the waterline, ground motions vary roughly linearly with nearshore swell wave energy.

[9] Ground tilt maps part of the vertical gravitational acceleration onto the observed horizontal component of ground motions [*Rodgers*, 1968]. Tilt effects increase with increasing period, and can contribute significantly to horizontal accelerations at infragravity frequencies [*Webb and Crawford*, 1999; *Crawford and Webb*, 2000]. *Young et al*. [2012] found near the cliff edge, ground tilt dominates the observed large (relative to vertical) cross-shore acceleration at infragravity frequencies (0.01–0.04 Hz), contributes significantly to cross-shore acceleration at swell frequencies (0.04–0.1 Hz), and is a small fraction of cross-shore acceleration at higher frequencies (0.2–0.5 Hz). Ground tilt is therefore an important feature in seismic records at coastal cliffs, and horizontal channels should be not interpreted as pure ground acceleration.

[10] Here, we compare near-shoreline seismic observations (0.01–40 Hz) from sites in California, Hawaii, North Carolina, Australia, and New Zealand (Figure 1), to explore whether previous observations and generation of coastal ground motions are consistent across more varied coastal settings and investigate the potential use of these observations in coastal studies.

3. Sites and Methods

[11] The eight shoreline sites (Figure 1 and Table 1) described below (sections 3.1–3.4) have been grouped according to site setting and morphology (California composite cliffs, cliffs fronted by elevated platforms, basalt cliffs, and beaches). Four of the shoreline sites (Del Mar, Point Loma, Imperial Beach, and Cardiff) are located within a 50 km coastal section of San Diego County, California, where the tide range is about 2 m. Concurrent observations were made at Point Loma and Imperial Beach.

3.1. Southern California Composite Cliffs

[12] *Del Mar, California, USA*: DELMAR (Figure 1b, described by *Young et al*. [2011]) is a 24 m cliff composed

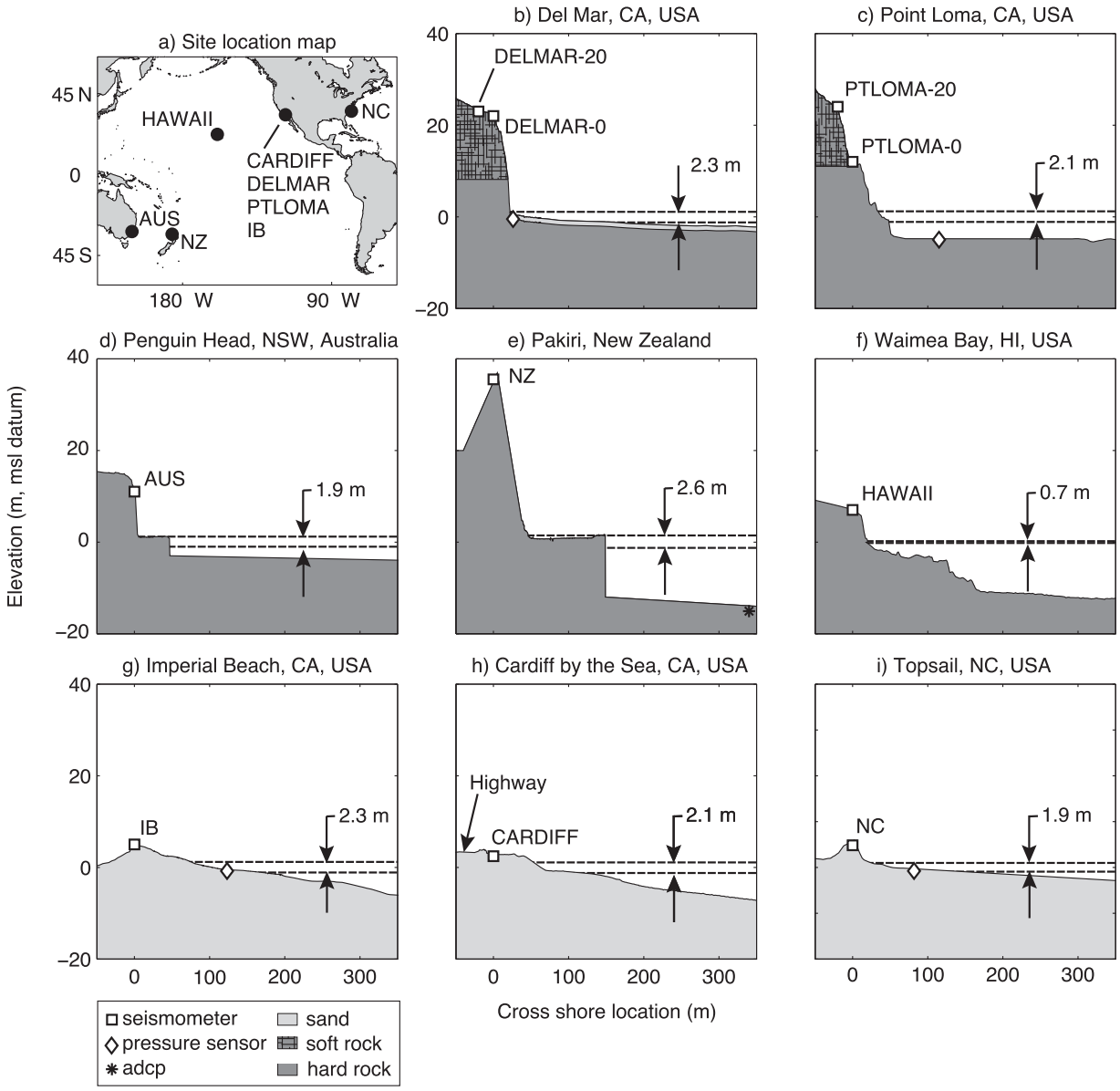

Figure 1. (a) Study site locations and (b–i) cross-shore profiles showing instrumentation, substrate (shading), and tidal range during the study period (dashed lines). Elevations (Figures 1b–1i) are relative to mean sea level (msl).

of well-cemented Eocene sedimentary deposits overlaid by a weakly cemented sandy Pleistocene terrace deposit. The cliff is fronted by a narrow sand (and occasionally cobble) beach, which is often flooded during high tides. At spring low tide, the waterline is more than 100 m offshore from the cliff base. The underlying shore platform is gently sloping and relatively smooth near the shoreline, but becomes somewhat irregular offshore forming several nearshore reef structures. Ground motions were observed at the cliff top edge (DELMAR-0) from 20 February 2010 to 2 April 2010 and 20 m inland from the edge (DELMAR-20) 29 November 2010 to 27 December 2010. Nearshore waves were monitored at the cliff base with a pressure sensor located on the shore platform under the beach about 4 m shoreward of the cliff base.

[13] *Point Loma, California, USA*: PTLOMA (Figure 1c) in Cabrillo National Monument (approximately 35 km south of DELMAR) is a 24 m high cliff composed of lithified Cretaceous sandstone and shale overlaid by a weakly cemented sandy Pleistocene terrace deposit. The cliff is fronted by a submerged shore platform that extends offshore forming reef structures. There is no fronting beach and waves are in continuous contact with the cliff. Ground motions were observed at a lower cliff location about 10 m above mean sea level (PTLOMA-0, 38 m inland from the waterline) and 20 m further inland on the cliff top (PTLOMA-20) from 5 August 2011 to 24 September 2011 and 22 August 2011 to 12 October 2011, respectively. Nearshore waves were monitored with a pressure sensor located on the submerged shore platform approximately 80

Table 1. General Site Characteristics and Instrumentation

Location	Coastal Setting	Foreshore	Seismometer Location	Estimated Distance to Waterline (m)	Tide Range[a] (m)	Incident Waves	Surfzone Waves	Start Date	End Date	Number of Days
Del Mar, CA, USA (DELMAR-0)	Cliff, 24 m, Eocene sedimentary overlaid by Pleistocene terrace deposits	Semi-submerged platform and beach	Cliff top	22–45	2.3[b]	Buoy[c] MOP	Pressure sensor	20 Feb 2010	2 Apr 2010	42
Del Mar, CA, USA (DELMAR-20)	Cliff, 24 m, Eocene sedimentary overlaid by Pleistocene terrace deposits	Semi-submerged platform and beach	Cliff top	42–65	2.3[b]	Buoy[c] MOP	Pressure sensor	29 Nov 2010	27 Dec 2010	29
Point Loma, CA, USA (PTLOMA-0)	Cliff, 24 m, Cretaceous sedimentary overlaid by Pleistocene terrace deposits	Submerged platform	Cliff base	38	2.1[b]	Buoy[c] MOP	Pressure sensor	5 Aug 2011	24 Sep 2011	51
Point Loma, CA, USA (PTLOMA-20)	Cliff, 24 m, Cretaceous sedimentary overlaid by Pleistocene terrace deposits	Submerged platform	Cliff top	58	2.1[b]	Buoy[c] MOP	Pressure sensor	22 Aug 2011	12 Oct 2011	52
Penguin Head, NSW, Australia (AUS)	Cliff, 15 m, Permian sedimentary	Elevated platform (40 m wide)	Mid Cliff	47 (5–47)[d]	1.9[e]	Buoy[e]		22 Nov 2011	12 Dec 2011	21
Pakiri, New Zealand (NZ)	Cliff, 37 m, Miocene sedimentary	Elevated platform (100 m wide)	Cliff top	149 (46–149)[d]	2.6	ADCP		17 Feb 2012	27 Mar 2012	40
Waimea Bay, HI, USA (HAWAII)	Cliff/low terrace, 8 m, Basalt, Koolau flow, 2–3 my in age	Rocky, submerged reef	Cliff top	20–22	0.7[b]	Buoy[c]		23 Dec 2011	5 Jan 2012	14
Imperial Beach, CA, USA (IB)	Dune, 6 m, unlithified sand	Beach	Dune top	75–165	2.3[b]	Buoy[c] MOP	Pressure sensor	29 Jul 2011	12 Sep 2011	46
Cardiff, CA, USA (CARDIFF)	Developed lagoon barrier, unlithified sand	Beach	Back Beach	40–120	2.1[b]	Buoy[c] MOP		21 Dec 2012	2 Jan 2013	13
Topsail, NC, USA (NC)	Dune, 6 m, unlithified sand	Beach	Dune top	17–75	1.9[b]	Buoy[c]	Pressure sensor	8 May 2012	23 May 2012	16

[a]Observed tide range during study period.
[b]Source: http://tidesandcurrents.noaa.gov/.
[c]Source: http://cdip.ucsd.edu/.
[d]Occasionally variable during high water levels.
[e]Source: Manly Hydraulics Laboratory (MHL) & NSW Office of Environment and Heritage's (OEH).

m offshore (118 m from the lower cliff seismometer), in a mean water depth of ∼5 m.

3.2. Australasian Cliffs Fronted by Elevated Shore Platforms

[14] *Penguin Head, New South Wales, Australia*: AUS (Figure 1d), a 15 m cliff situated on a headland composed of lithified Permian Wandrawandian siltstone (upper Shoalhaven group), is fronted by a 40 m wide elevated (near Mean High Water) shore platform. The 3–4 m water depth at the seaward edge of the platform allows energetic incident waves (broken and unbroken) to interact with the shore platform. Ground motions were observed approximately mid cliff. Seismic data 130 km inland of the cliff obtained from the CNB Australian National Seismic Network seismometer (http://www.ga.gov.au/earthquakes/seismicSearch.do) were analyzed and used for comparison.

[15] *Pakiri, New Zealand*: NZ (Figure 1e, described by *Dickson and Pentney* [2012]) is a 37 m cliff composed of the Pakiri Formation (Waitemata Group), with gently landward dipping beds of coarse, medium, and fine sandstone and sandy mudstone. The cliff is fronted by an extensive 100 m wide elevated (near Mean High Water Springs) shore platform. The 12 m water depth seaward of the platform edge exposes the platform zone to unbroken incident waves. At the platform edge, depending on tide and wave conditions, incident waves were reflected, surged onto the platform, or broke. Data from the WCZ New Zealand National Seismograph Network (http://www.geonet.org.nz/) seismometer located 10 km inland and 50 km northwest of the cliff site were analyzed. Nearshore waves and water levels (tide range ∼2.6 m) were monitored with an ADCP (Acoustic Current Doppler Profiler—Workhorse Monitor/Sentinel) deployed approximately 200 m off the seaward edge in 15 m water depth.

3.3. Hawaiian Basalt Cliffs

[16] *Waimea Bay, Hawaii, USA*: HAWAII (Figure 1f) is an 8 m terrace set on a rocky point composed of ∼2 million year old basalt. The site is fronted by a submerged platform/reef structure covered by boulders and exposed to famously energetic swell during northern hemisphere winter [*Vitousek and Fletcher*, 2008]. There is no fronting beach and waves are in continuous contact with the seaward terrace edge. The tide range is small, about 0.7 m. Ground motions were observed near the terrace edge, 20 m from the waterline. Seismic data from the Kipapa (KIP) global seismograph network seismometer, located 25 km inland of the cliff site, were obtained from IRIS (http://www.iris.edu/dms/dmc/) and analyzed.

3.4. Beaches

[17] *Imperial Beach, California, USA:* IB (Figure 1g, approximately 45 km south of DELMAR) is a sandy beach backed by a 6 m dune composed of loose sand. Ground motions were observed near the dune crest. The site lacks rocky substrate and nearshore reefs. Surfzone waves were monitored with a pressure sensor located 82 m seaward of the seismometer, in a mean water depth of ∼1 m. At low tide, the pressure sensor was occasionally above the waterline.

[18] *Cardiff by the Sea, California, USA:* CARDIFF (Figure 1h, approximately 5 km north of DELMAR) is a sandy beach backed by riprap, a highway, and other infrastructure, set on a lagoon barrier. Ground motions were observed in the back beach of a recently placed beach fill about 25 m seaward of the highway and about 50 m from the upper shoreface. The site lacks rocky substrate and nearshore reefs.

[19] *Topsail, North Carolina, USA*: NC (Figure 1i) is a 6 m dune composed of loose sands fronted by an extensive beach. The site lacks rocky substrate and nearshore reefs. The tide range is about 2 m. Ground motions were observed near the dune crest. Seismic data from the CNNC Advanced National Seismic System (http://earthquake.usgs.gov/monitoring/anss/) located 90 km inland were also analyzed.

3.5. Seismometers

[20] Ground motions at all sites were measured at 100 Hz with a Nanometrics Compact Trillium broadband velocity seismometer for at least 13 days. Sensors were installed and buried approximately 90 cm from the ground surface. The seismometer response has 3 dB corners at 0.0083 and 108 Hz. The raw velocity data were phase and magnitude corrected in the frequency domain according to the instrument response curve for frequencies above 0.005 Hz (lower frequencies are not investigated in this study). Seismic data, divided into 1 h epochs, were detrended and processed with standard Fourier spectral methods [*Jenkins and Watts*, 1968]. One hour records containing significant ground motion from earthquakes, post installation settlement, or local noise were identified by comparison with inland data and removed manually. Seismic data were band-passed into infragravity (IG), single (SF), double (DF), and two high frequency (HF1 and HF2) bands for analysis. Infragravity and single frequency band limits (Table 2) were selected based on site incident ocean wave frequencies. Double frequency band limits were estimated by comparing energy spectra with inland observations. High-frequency site spectra occasionally displayed distinct frequency bands with elevated signals and variable temporal patterns. At each site, the two most visually distinct bands were assigned HF1 and HF2 band limits accordingly. Horizontal seismic data at HAWAII was compromised, precluding some analyses. High-frequency noise (∼25 Hz) at CARDIFF from a nearby gasoline generator was removed. At the San Diego County shoreline sites, observations from the Camp Elliot (CPE) Broadband Seismic Data Collection Center network seismometer located 14 km inland were included to compare with the coastal data and provide levels of nonlocal background noise (http://eqinfo.ucsd.edu/deployments/anza/index.php).

3.6. Incident Wave Conditions

[21] At the San Diego County shoreline sites (DELMAR, PTLOMA, IB, CARDIFF), a wave buoy network (http://cdip.ucsd.edu) was used to estimate hourly significant wave height at virtual buoys or "Monitored and Prediction" points (MOPS) in 10 m depth. The effects of complex offshore (e.g., the Channel Islands of California) and local bathymetry on ocean swell were simulated with a spectral refraction wave model initialized with offshore buoy data [*O'Reilly and Guza*, 1991]. At DELMAR, PTLOMA, and IB, nearshore waves and runup were observed with

Table 2. Site Frequency Band Limits (Hz)

	IG		SF		DF		HF1		HF2	
Site	Min	Max	Min	Max	Min	Max	Min	Max	Min	Max
DELMAR	0.01	0.03	0.04	0.09	0.10	0.4	0.5	2	5	30
PTLOMA	0.01	0.03	0.04	0.09	0.10	0.4	0.5	2	5	30
AUS	0.01	0.03	0.04	0.09	0.10	0.4	0.5	2	2	40
NZ	0.01	0.03	0.04	0.10	0.14	0.4	2.0	10	10	30
HAWAII	0.01	0.03	0.04	0.10	0.10	0.6	2.0	6	9	20
IB	0.01	0.03	0.04	0.09	0.10	0.4	0.5	2	5	30
CARDIFF	0.01	0.03	0.04	0.20	0.25	0.6	1.0	6	7	20
NC	0.01	0.03	0.04	0.20	0.25	0.6	0.7	2	5	30

Paroscientific pressure sensors (model 245A-102, subcentimeter accuracy), sampling at 8 Hz, buried in the beach or attached to the shore platform. Pressure observations were processed by removing atmospheric pressure, correcting for clock drift, detrending, and converting to hydrostatic elevation. At all shoreline sites, except NZ (where the ADCP provided incident wave data), hourly buoy data (Table 1) were analyzed. Incident wave conditions were generally moderate with Hs in the range 0.5–2.0 m. Waves exceeded 3 m only at HAWAII.

3.7. Data Analysis

[22] Signal coherence and phase differences were calculated using standard cross-spectral analysis [*Jenkins and Watts*, 1968]. Coherence above 95% confidence level was considered significant. Mean hourly direction (or principal axis) of low-frequency horizontal signals (primarily ground tilt signals) was computed from principal component analysis using the two horizontal channels and shows the predominant planimetric tilt/loading direction. Estimates of directional mean spread are based on methods used to estimate directional spread in ocean waves using buoy observations of horizontal tilts [*Kuik et al*., 1988]. Spread is defined here as the half-width of a top-hat directional distribution centered on the mean direction giving horizontal statistics similar to those observed [*Herbers et al*., 1999]. Spread of 0°, 45°, and 180° indicate that all tilt is in one (principal) axis, most of the tilt is within 45° of the principal axis, and the tilt on major-minor axes is equal, respectively.

4. Observations

4.1. Vertical Infragravity Frequency

[23] At all eight shoreline sites (Figure 1), locally generated infragravity (0.01–0.03 Hz) ground motion was orders of magnitude above inland levels, and increased with increasing incident wave energy and tidal water level (Figures 2–5), consistent with previous studies [*Young et al*., 2011, 2012]. Excluding nonlocal double frequency microseisms, infragravity frequencies had the highest energy levels in the vertical velocity spectrum at most shoreline sites (Figure 6a). Although the infragravity bandwidth is narrow (0.02 Hz, Table 2), the velocity variance is also dominated by infragravity motions. The largest observed incident ocean waves at Hawaii (significant height 4–5 m) produced the largest vertical ground displacements (amplitudes of several mm, Figure 2f), primarily from infragravity band motions that also dominated displacements at all other shoreline sites.

[24] Locally generated infragravity ground motions and tide level were significantly correlated (>95% confidence level) at all shoreline sites and were maximum at high tide (Figure 5) except HAWAII, where there was a 50° phase shift of unknown origin. The tidal dependence dominates the infragravity (IG) variability compared to incident waves at the beach sites (R^2 for IG energy and tide ranged 0.48–0.69 versus 0.07–0.27 for incident waves, Figure 5), probably because the distance from the waterline to the seismometers at low tide was often more than double the distance at high tide (Figure 1).

4.2. Vertical Single Frequencies

[25] At all eight shoreline sites, locally generated single frequency ground motion was elevated above inland levels, and increased with increasing incident wave energy (Figures 2–4). At all shoreline sites except Australasian cliffs, single frequency ground motion was significantly tidally modulated. Single frequency signals at HAWAII exhibited 20° phase shifts compared to tide, similar to infragravity signals.

4.3. Vertical Double Frequencies

[26] At all sites, vertical double frequency spectral levels at the coast and inland were nearly identical (Figures 2–4 and 6b), consistent with a common (distant or spatially distributed) source [e.g., *Young et al*., 2011]. Double frequency ground motion was tidally modulated at some shoreline sites, probably from frequency overlap with the tidally modulated single frequency.

4.4. Vertical High Frequencies

[27] At all eight shoreline sites, high frequency ground motion was elevated above inland levels, and increased with incident wave energy (Figures 2–4). At all shoreline sites except HAWAII and NC, high-frequency motion was significantly coherent (>95% confidence) with tide and generally elevated at higher tides (e.g., Figures 2b and 2c). Small tide changes at HAWAII and local noise at NC may have caused the lack of tidal modulation. At NZ, high frequency ground motion increased at low-midtides (Figures 4a and 4b), consistent with previous observations at this site [*Dickson and Pentney*, 2012].

4.5. Horizontal Infragravity Signals (Tilt) and Directional Analysis

[28] Mean tilt direction was generally consistent with the estimated cross-shore orientation (NC, Figure 7a). However, at NZ the mean direction deviates about 50° from cross-shore between 18 and 26 March, and then

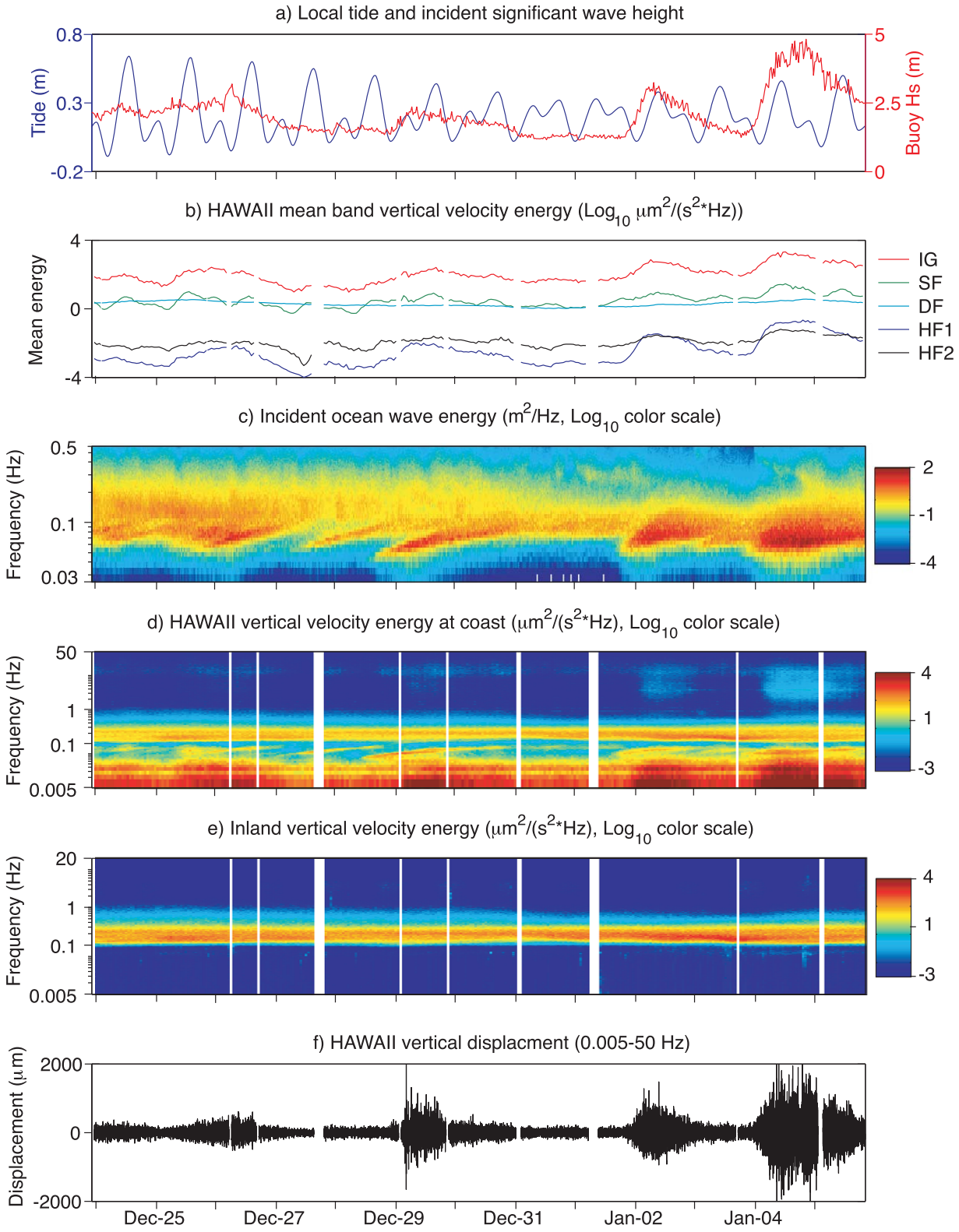

Figure 2. Waimea Bay (HAWAII): (a) tide elevation and buoy significant wave height and (b) log band-averaged spectral density of vertical ground velocity versus time. Color plots are log (see scales): (c) buoy wave energy spectral density; and vertical velocity energy density, (d) at the coast (HAWAII) and, (e) 25 km inland (KIP) versus frequency and time, and (f) HAWAII vertical displacement (all frequency bands) versus time. Data gaps are from manually removed 1 h records containing significant noise.

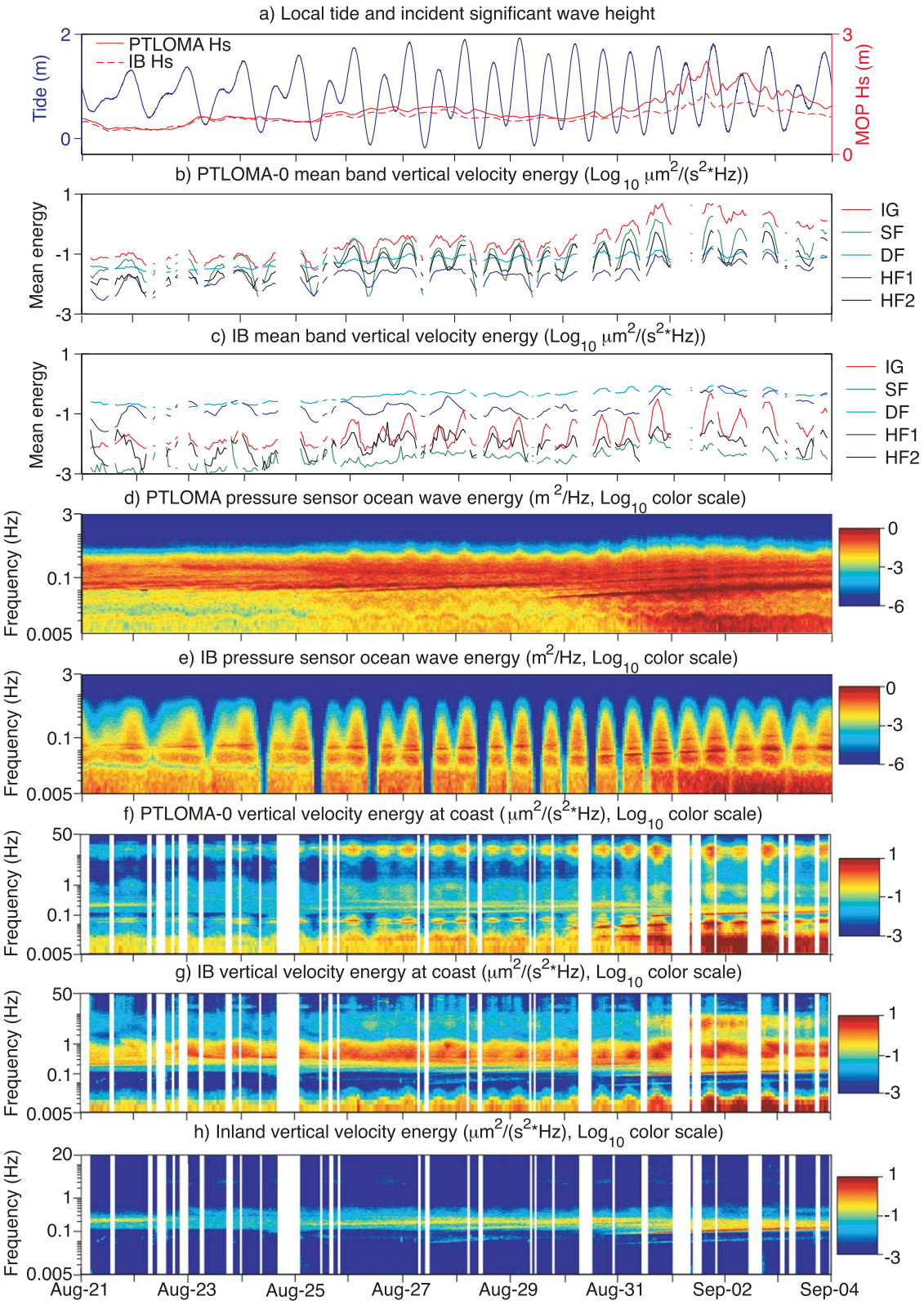

Figure 3. Time series at Point Loma (PTLOMA) and Imperial Beach (IB) of (a) tide elevation and significant wave height (10 m water depth); band-averaged log spectral density of vertical ground velocity for (b) PTLOMA-0 and (c) IB. Color plots (see log scale) are nearshore pressure sensor spectral density for (d) PTLOMA and (e) IB, and vertical velocity energy density versus log frequency and time at the coast (f) PTLOMA-0, (g) IB, and (h) 14 km inland (CPE). Data gaps are from manually removed 1 h records containing significant noise (e.g., earthquakes).

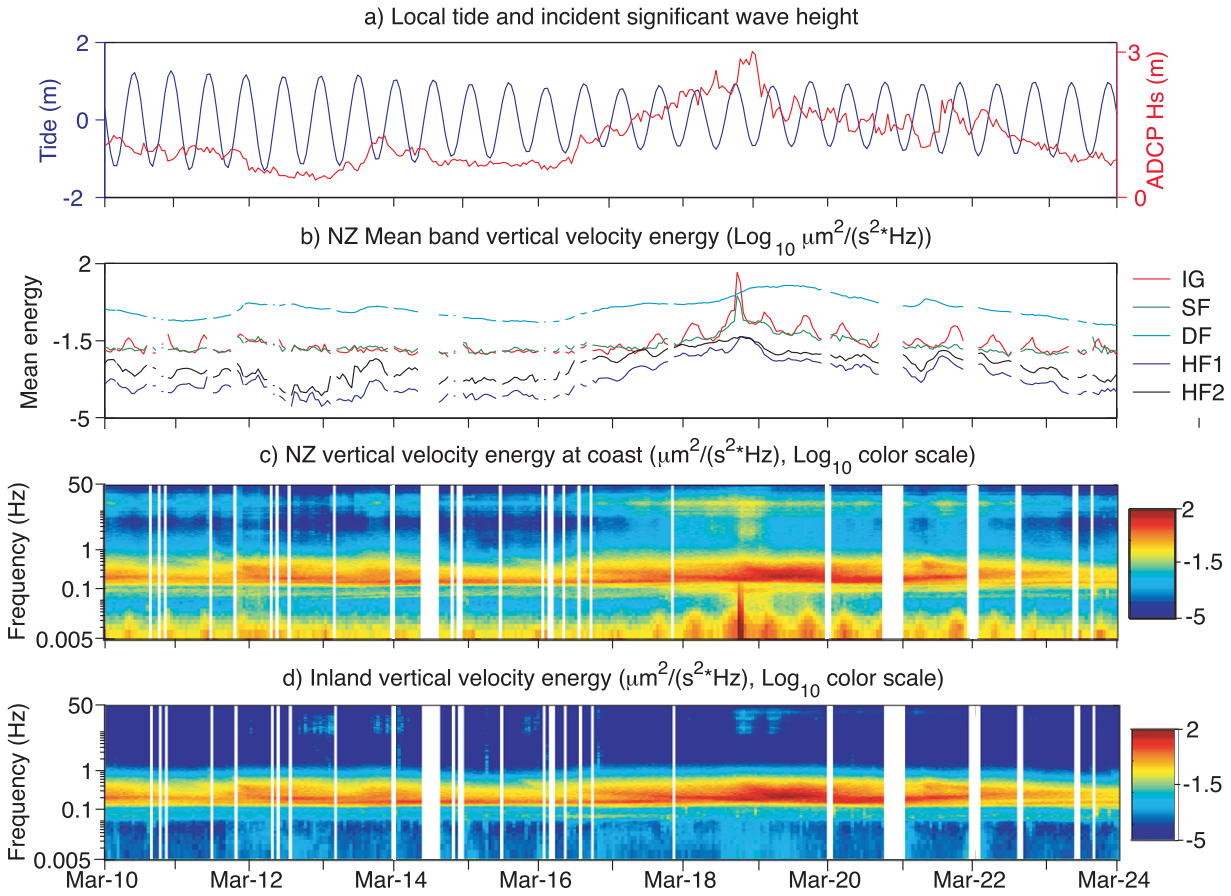

Figure 4. Pakiri (NZ): (a) tide elevation and significant wave height (15 m water depth) and (b) band-averaged log spectral density of vertical ground velocity, both versus time. Colors plots (see scale) are log vertical velocity energy density versus log frequency and time: (c) at the coast (NZ) and (d) 10 km inland (WCZ). Data gaps are from manually removed 1 h records containing significant noise.

reapproaches cross-shore orientation (Figure 7b). Mean direction was significantly coherent (>95% confidence) with tide at PTLOMA-0, NC (Figure 7a), and IB.

[29] Directional spread varied between shoreline sites, and over time at each site, but was generally between 30° and 150° (Figure 7). Directional spread increased inland at

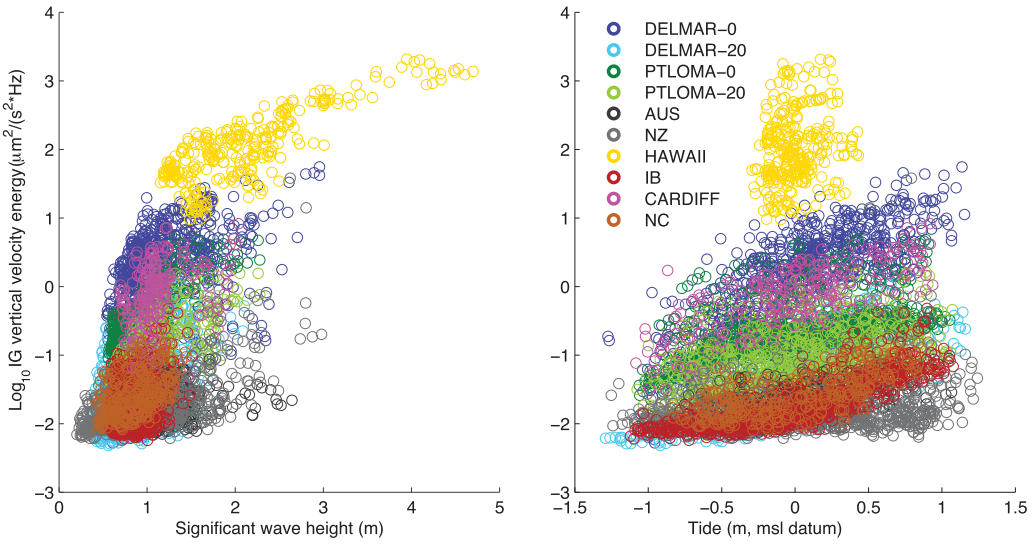

Figure 5. Hourly log vertical infragravity velocity energy density versus (left) local significant incident wave height and (right) tide elevation.

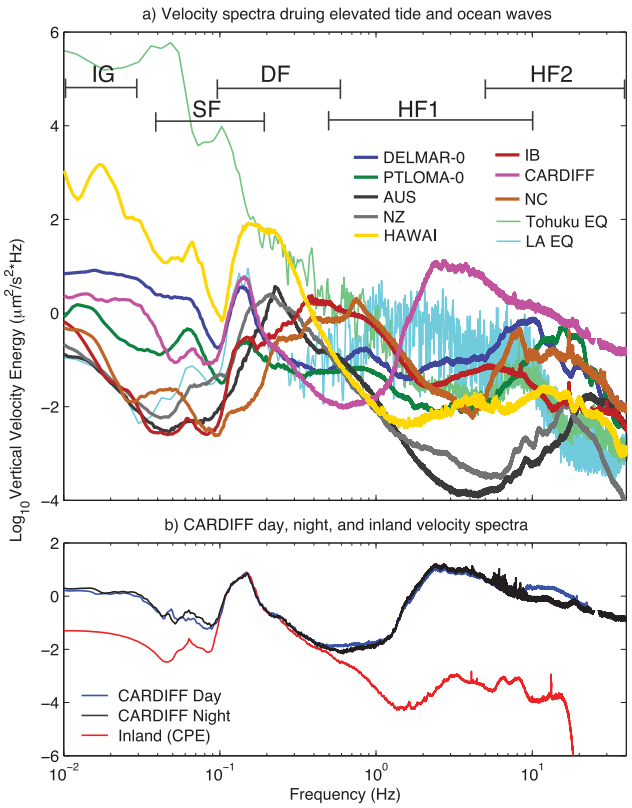

Figure 6. (a) Log vertical velocity spectral density versus frequency for eight sites and two earthquakes (see legend). At each site, the average is shown (outliers removed) for cases with relatively energetic ground motions (e.g., when incident waves are larger than the site median, and tide is above mean sea level). Earthquake spectra from ground motion recorded at DELMAR of a local (4.4 Los 37 Angeles, distance 135 km, 16 March 2010, 11:04 UTC) and nonlocal earthquake (9.0 Tohuku, distance 8500 km, 11 March 2011, 5:46 UTC) are also shown. Approximate ranges of infragravity (IG), single (SF), double (DF), and high frequency (HF1 and HF2) bands are indicated (see Table 2 for specific ranges at each site). (b) CARDIFF vertical velocity spectra during daytime traffic (blue) and nighttime nontraffic conditions (black), and nonlocal noise background (inland, CPE).

DELMAR and PTLOMA. Spread was significantly coherent (>95% confidence) with tide and (within 20° of) in phase at PTLOMA-0, PTLOMA-20, and IB, and out of phase at DELMAR-20 and NZ with phase differences of 180° and 40°, respectively.

4.6. Comparison With Traffic Noise and Earthquakes

[30] Comparisons of locally ocean-generated seismic energy with earthquakes and local traffic noise provide scale for the observed coastal motion. Ground motions at DELMAR-0 during a strong distant earthquake (9.0 Tohuku, distance 8500 km, 11 March 2011, 5:46 UTC) are elevated three orders of magnitude above typical levels at infragravity frequencies, and by 10^2 at single frequencies (Figure 6a). A local earthquake (4.4 Los Angeles, distance 135 km, 16 March 2010, 11:04 UTC) did not significantly alter the DELMAR-0 hourly spectra (Figure 6a), although residents near DELMAR reported feeling "weak" shaking (earthquake.usgs.gov/earthquakes/dyfi/) from the earthquake. The wave-induced motions are at least comparable in magnitude to this local earthquake, which suggests they can also be felt, and is consistent with clifftop residents reporting ocean wave related shaking. At CARDIFF, daytime traffic (generated 25 m away, including heavy trucks) slightly elevates ground motion (Figure 6b) at higher frequencies around 10–20 Hz. At lower infragravity and single frequencies (0.01–1 Hz), local traffic noise appears insignificant and the signals are dominated by local ocean generation.

5. Discussion

5.1. Tidal and Morphological Influence

[31] These short-term observations of locally ocean-generated coastal ground motion are generally consistent with previous studies [*Adams et al*., 2002, 2005; *Young et al*., 2011, 2012], and at most shoreline sites ground motion was tidally modulated with relatively more motion during high tide. However, variations of tidal influence point toward important differences in site morphological controls and local coastal processes. For example, although AUS and NZ are broadly similar with elevated shore platforms, shaking at AUS is elevated at high tide, not mid-low as at NZ. Water depths offshore of the platforms probably cause the difference. At AUS shallow water depths cause wave shoaling and breaking prior to wave-platform interaction. Similar to other shoreline sites, the sloping bottom causes tidal modulation of wave dissipation with more energy closer to land during high tide. At NZ, the deeper water allows waves to approach the platform without much tidal change in dissipation, and at lower tides shaking increases from more waves breaking into the platform edge as opposed to surging on top during higher tide levels. This restricts wave induced shaking to a more tidally constrained time period.

[32] Morphological control of ground motion is further demonstrated by signal directionality. The mean direction at NZ deviated from cross-shore (Figure 7b) during a period of relatively large incident waves and realigned with a sizeable channel/gap in a section of the shore platform, raising the possibility that the shore platform may exert control over low frequency wave runup and loading. Directional spread was tidally influenced at some shoreline sites, but overall spread behavior was inconsistent across sites.

[33] While all shoreline sites exhibit tidally modulated infragravity signals, NZ and AUS lack a tidally modulated single frequency ground motion signal, possibly because the elevated shore platforms limit single frequency wave runup, and single frequency signals generated shoreward of the platform are substantially decayed at the cliff. Alternatively, single frequency waves could dissipate or transform to infragravity frequencies over the shore platform as observed elsewhere [*Stephenson and Kirk*, 2000; *Beetham and Kench*, 2011; *Marshall and Stephenson*, 2011; *Ogawa et al*., 2011; *Ogawa*, 2012]. These findings further demonstrate that platform morphology influences ocean energy delivery to the cliffs, as noted in previous studies [*Lim et al*., 2011; *Dickson and Pentney*, 2012], and focuses

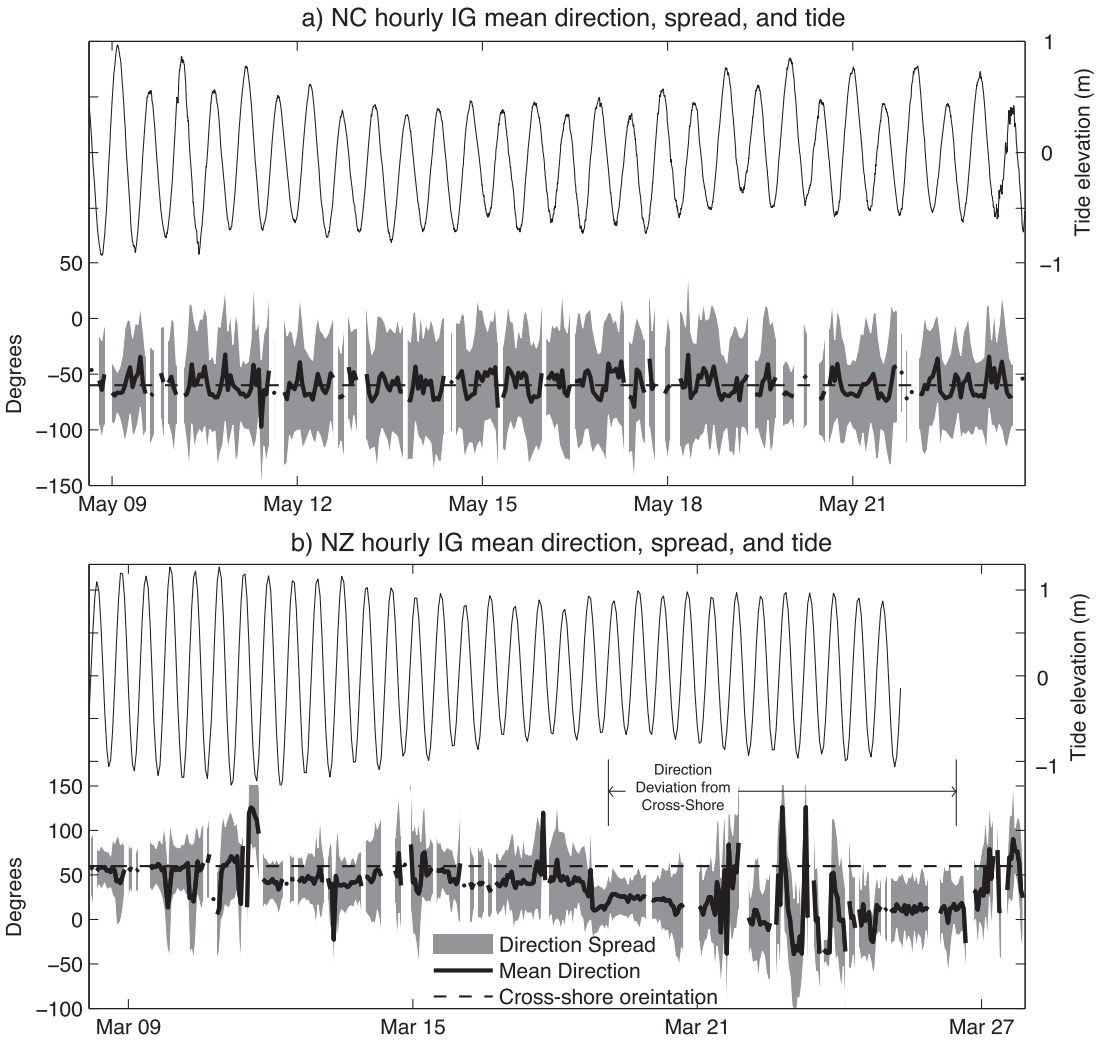

Figure 7. Time series of hourly horizontal infragravity band (signals primarily from tilt) mean direction (thick solid line) and directional spread (gray region) for (a) NC and (b) NZ. Dashed line is the estimated cross-shore orientation. Sites DELMAR-0, DELMAR-20, PTLOMA-0, PTLOMA-20, IB, AUS, and CARDIFF (not shown) are similar to Figure 7a.

attention on the possible role of infragravity waves in rock coast, cliff, and platform processes [*Dickson et al*., 2013].

[34] Concurrent observations at nearby IB and PTLOMA (Figure 3) offer a comparison of different lithology/setting (beach and cliff) exposed to similar incident offshore waves and illustrate different flexing and high-frequency responses. Although shaking at IB was tidally modulated, it was more pronounced at PTLOMA despite relatively larger tidal modulation of pressure sensor data at IB. Larger incident waves at PTLOMA helped to generate large flexing motions compared to IB.

5.2. Composition Influence

[35] High frequency (0.5–40 Hz) ground response varied between shoreline sites but consistently exhibited one or more frequency ranges with elevated response (Figure 8). At some shoreline sites, such as NZ, the elevated response peaked over a relatively narrow range (15–17 Hz), while at other sites, such as AUS, the elevated response was broader (Figure 8). Similar high frequency response peaks at 7–10 Hz occurred at DELMAR-0, DELMAR-20, and PTLOMA-20, where the seismometers were all deployed in Quaternary terrace deposits. Shoreline sites composed of softer material and/or loose sands had elevated motion at lower frequencies compared to sites with older, harder material, possibly from more effective high-frequency damping in the softer materials. Recently placed loose sand at CARDIFF may have contributed to larger high-frequency ground motion compared to other beach sites, because the sand was relatively uncompacted and subject to settling.

[36] PTLOMA vertical cliff ground motion decayed with distance inland and band energies at the cliff top and cliff base were coherent and in phase. However, the high-frequency peaks (Figure 8) were dissimilar and the PTLOMA-0 peak was about 10 Hz higher than PTLOMA-20, probably because of differences in substrate (Figure 1). NZ and AUS are similar in lithology and morphology, however the variable high-frequency response suggests modest local site differences can cause substantially

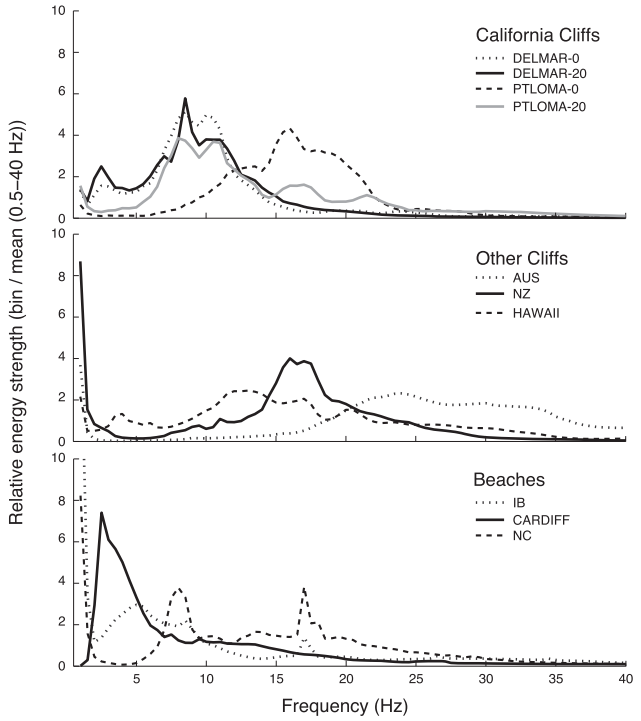

Figure 8. Relative strength of high-frequency vertical velocity signal for 0.5 Hz bins (ratio of bin energy to the hourly mean over the 0.5–40 Hz range).

different high-frequency responses. These results suggest local geologic conditions, substrate, and resonance probably influence the high-frequency response spectra.

5.3. Inland Signal Decay

[37] Ocean-generated cliff motion decayed inland at PTLOMA and DELMAR, where sensors were deployed on a cross-shore transect, consistent with previous studies [*Adams et al*., 2005; *Dickson and Pentney*, 2012; *Young et al*., 2012]. Low-frequency seismic minima at low tide, at a fixed sensor, also suggest inland decay at other shoreline sites because the loading source moves offshore during decreasing tides. *Adams et al*. [2005] suggested cliff motion decay might cause cliff weakening through strain-related fatigue processes and provide a related model. Low-frequency cliff strains on the order of 10^{-6} have been observed at DELMAR [*Young et al*., 2012] and in Santa Cruz, California [*Adams et al*., 2005]. Displacement observations at HAWAII of several mm (Figure 2f) suggest strain magnitudes can reach much higher levels, however more research is needed to assess the possibility of rock damage from coastal flexing.

5.4. Geomorphic Proxy and Modeling Flexing Motion

[38] Wave-cliff interactions are poorly understood, partly because the environment makes field studies difficult and few quantitative observations exist. Seismic observations at coastal cliffs provide a potential alternative method to monitoring wave-cliff interaction and a potential proxy for wave forcing on coastal cliffs. However, site comparison of high frequency motion reveals complications that must be addressed. Observations indicate breaking ocean waves on a sandy beach cause high-frequency ground motions similar to wave-cliff impacts. Comparison of traffic noise and ocean generated signals at CARDIFF indicate local noise sources can also generate relatively large high-frequency ground motions. More research is needed to potentially separate different mechanisms causing high-frequency signals before this proxy can be easily used.

[39] *Young et al*. [2012] developed a simple empirical model relating vertical infragravity cliff motion at DELMAR to incident swell wave energy and the seismometer-to-waterline distance (a proxy for ocean wave loading and attraction). At PTLOMA, the seismometer-to-waterline distance is fixed, but the seismic observations were still tidally modulated, indicating that water levels influence the ocean wave energy and resulting loading. Decreased loading during lower tides is probably from increased wave dissipation associated with shoaling on the submerged reef. This suggests wave loading is influenced by local ocean wave transformation and site characteristics in addition to loading distance, and at PTLOMA or similar shoreline sites, water level can be a more robust proxy than seismometer-to-waterline distance. These observations show that using a simple proxy such as water level or distance-to-waterline is inappropriate at some shoreline sites and makes direct cross-site comparisons difficult. Modeling is also complicated by variable signal decay rates at different sites. These issues will need to be resolved before a uniform proxy for marine forcing can be established.

6. Summary

[40] Ground motions observed at eight sites on rocky, cliffed, and sandy shorelines were consistently generated by local ocean waves and elevated above inland motion levels in two main frequency ranges. Between about 0.01 and 0.1 Hz, the foreshore loading and gravitational attraction from runup of individual ocean swell and infragravity waves drives coherent, in phase, flexing motion that decays inland. Directional analysis shows the associated low-frequency ground tilt is generally oriented cross-shore. At higher frequencies, between 0.5 and 40 Hz, coastal shaking is observed at all shoreline sites, including sandy beaches lacking cliffs and platforms, indicating shaking can be generated by general wave breaking processes, as well as by wave-cliff and wave-platform impacts. Seismic observations are therefore not a simple proxy for wave-cliff and wave-platform interactions, and additional research is needed to separate the high-frequency contributions from breaking waves not impacting the cliff or platform.

[41] Overall energy spectra between shoreline sites were generally consistent and usually within a few orders of magnitude of one another, despite the different coastal settings and site compositions. However, specific site seismic response to local ocean waves varied and was influenced by tide level, incident wave energy, site morphology, composition, and signal decay. The frequencies of elevated peaks between 0.5 and 40 Hz varied between shoreline sites, possibly related to local site geometry and ground material properties. Flexing and shaking both increased with incident wave energy and was often tidally modulated, consistent with local generation. Shoreline sites differ in the tide phase with maximum ground motions, illustrating that local morphology can influence ground motions.

Relatively similar spectral shapes at some shoreline sites support site composition and setting influences on the seismic response.

[42] **Acknowledgments.** California Department of Boating and Waterways, and the U.S. Army Corps of Engineers, as part of the Coastal Data Information Program (CDIP) sponsored primary wave data collection. A.P.Y. received research support from the California Department of Boating and Waterways Oceanography Program. The California Energy Commission PIER program partially funded the field observations. We gratefully thank the Del Mar Beach Club, the Solana Beach Lifeguards, the Jacobs family, Keith Lombardo, Benjamin Pister, the Brady family, Colin Woodroffe, the Manly Hydraulics Lab, and NSW Office of Environment and Heritage, Camp Surf, Michele Okihiro, Greg Schmidt, Martin and Jan Munro, Brendan Hall, Jim Mensching, and Jessica Carilli for their assistance and support. Engineer Brian Woodward, his staff, and Julia Fiedler contributed substantially to the data collection.

References

Adams, P. N., R. S. Anderson, and J. Revenaugh (2002), Microseismic measurement of wave-energy delivery to a rocky coast, *Geology*, *30*(10), 895–898.

Adams, P. N., C. D. Storlazzi, and R. S. Anderson (2005), Nearshore wave-induced cyclical flexing of sea cliffs, *J. Geophys. Res.*, *110*, F02002, doi:10.1029/2004JF000217.

Agnew, D. C., and J. Berger (1978), Vertical seismic noise at very low frequencies, *J. Geophys. Res.*, *83*(B11), 5420–5424, doi:10.1029/JB083iB11p05420.

Amitrano, D., J. R. Grasso, and G. Senfaute (2005), Seismic precursory patterns before a cliff collapse and critical point phenomena, *Geophys. Res. Lett.*, *32*, L08314, doi:10.1029/2004GL022270.

Amundson, J. M., J. F. Clinton, M. Fahnestock, M. Truffer, M. P. Lüthi, and R. J. Motyka (2012), Observing calving-generated ocean waves with coastal broadband seismometers, Jakobshavn Isbræ, *Greenland, Ann. Glaciol.*, *53*(60), 79–84.

Beetham, E. P., and P. S. Kench (2011), Field observations of infragravity waves and their behaviour on rock shore platforms, *Earth Surf. Processes Landforms*, *36*(14), 1872–1888.

Bossolasco, M., G. Cicconi, and C. Eva (1973), On microseisms recorded near a coast, *Pure Appl. Geophys.*, *103*(1), 332–346, doi:10.1007/BF00876409.

Bromirski, P. D., and R. A. Stephen (2012), Response of the Ross Ice Shelf, Antarctica, to ocean gravity-wave forcing, *Ann. Glaciol.*, *53*(60), 163–172.

Crawford, W. C., and S. C. Webb (2000), Identifying and removing tilt noise from low-frequency (<0.1 Hz) seafloor vertical seismic data, *Bull. Seismol. Soc. Am.*, *90*(4), 952–963, doi:10.1785/0119990121.

Dickson, M. E., and R. Pentney (2012), Micro-seismic measurements of cliff motion under wave impact and implications for the development of near-horizontal shore platforms, *Geomorphology*, *151*, 27–38.

Dickson, M. E., H. Ogawa, P. S. Kench, and A. Hutchinson (2013), Sea-cliff retreat and shore platform widening: Steady-state equilibrium?, *Earth Surf. Processes Landforms*, *38*(9), 1046–1048.

Herbers, T. H. C., S. Elgar, and R. T. Guza (1999), Directional spreading of waves in the nearshore, *J. Geophys. Res.*, *104*(C4), 7683–7693.

Jenkins, G. M., and D. G. Watts (1968), 525 pp. *Spectral Analysis and Its Applications*, Holden-Day, San Francisco, Calif.

Kuik, A. J., G. P. van Vledder, and L. H. Holthuijsen (1988), A method for the routine analysis of pitch-and-roll buoy wave data, *J. Phys. Oceanogr.*, *18*(7), 1020–1034.

Lim, M., N. J. Rosser, D. N. Petley, and M. Keen (2011), Quantifying the controls and influence of tide and wave impacts on coastal rock cliff erosion, *J. Coastal Res.*, *27*(1), 46–56.

Marshall, R. J., and W. J. Stephenson (2011), The morphodynamics of shore platforms in a micro-tidal setting: Interactions between waves and morphology, *Mar. Geol.*, *288*(1), 18–31.

Ogawa, H. (2012), Observation of wave transformation on a sloping type B shore platform under wind-wave and swell conditions, *Geo Mar. Lett.*, *33*(1), 1–11.

Ogawa, H., M. E. Dickson, and P. S. Kench (2011), Wave transformation on a sub-horizontal shore platform, *Cont. Shelf Res.*, *31*, 1409–1419.

O'Reilly, W. C., and R. T. Guza (1991), Comparison of spectral refraction and refraction-diffraction wave models, *J. Waterw. Port Coastal Ocean Eng.*, *117*(3), 199–215.

Rodgers, P. W. (1968), Response of horizontal pendulum seismometer to Rayleigh and Love waves, tilt, and free oscillations of Earth, *Bull. Seismol. Soc. Am.*, *58*(5), 1384–1406.

Senfaute, G., A. Duperret, and J. A. Lawrence (2009), Micro-seismic precursory cracks prior to rock-fall on coastal chalk cliffs: A case study at Mesnil-Val, Normandie, NW France, *Nat. Hazards Earth Syst. Sci.*, *9*, 1625–1641.

Stephenson, W. J., and R. M. Kirk (2000), Development of shore platforms on Kaikoura Peninsula, South Island, New Zealand: Part one: The role of waves, *Geomorphology*, *32*(1), 21–41.

Vitousek, S., and C. H. Fletcher (2008), Maximum annually recurring wave heights in Hawai'I, *Pac. Sci.*, *62*(4), 541–553.

Webb, S. C., and W. C. Crawford (1999), Long-period seafloor seismology and deformation under ocean waves, *Bull. Seismol. Soc. Am.*, *89*(6), 1535–1542.

Young, A. P., P. N. Adams, W. C. O'Reilly, R. E. Flick, and R. T. Guza (2011), Coastal cliff ground motions from local ocean swell and infragravity waves in southern California, *J. Geophys. Res.*, *116*, C09007, doi:10.1029/2011JC007175.

Young, A. P., R. T. Guza, P. N. Adams, W. C. O'Reilly, and R. E. Flick (2012), Cross-shore decay of cliff top ground motions driven by local ocean swell and infragravity waves, *J. Geophys. Res.*, *117*, C06029, doi:10.1029/2012JC007908.